Impact factors on the active power flow recovery in multi-terminal HVDC systems after DC fault clearing

C Brantl, P Tünnerhoff*, A Peitz*, A Schnettler**

**RWTH Aachen University, Schinkelstr. 2, 52056 Aachen, Germany, brantl@ifht.rwth-aachen.de*

Keywords: HVDC, multi-terminal, protection, recovery

Abstract

Multi-terminal HVDC systems have been proposed as a promising solution to enable the large-scale integration of offshore wind power plants. Due to the envisaged amount of installed generation capacity in the range of several gigawatts, a high availability of these DC grids is required, as a loss of power transfer from the HVDC grid to the AC grid could endanger the overall system stability. Consequently, a fast, and secure fault handling strategy for faults in the DC grid is needed. So far, no standard DC grid protection system is available for HVDC grids. Several fault clearing strategies have been proposed, with most publications focussing on selectivity and breaker design and stresses for the different fault clearing strategies. This paper shifts the focus to the power flow recovery after fault clearing to identify recovery times and the main impact factors on it. To this end, a selective fault clearing strategy based on HVDC circuit breakers is evaluated in PSCAD | EMTDC for varying fault scenarios and breaker opening times with regard to the recovery of the DC voltage and the active power transfer to the AC side. The results indicate, that fast fault clearing leads to a faster recovery, where changes in the range of few milliseconds in the fault clearing may have a huge impact on the power flow deviations.

1 Introduction

Worldwide the integration of offshore wind power is increasing. Current prognosis estimate 48 GW of installed capacity in the North Sea until 2030 [1]. Due to the long distance from shore, high voltage direct current (HVDC) transmission based on state-of-the-art Modular Multilevel Converters (MMC) will be applied for most of these wind farms. While the existing HVDC systems for connection of wind farms are point-to-point links, the construction of a meshed HVDC grid is discussed to (inter-)connect a high number of future wind farms [2]. This would lead to a new grid structure with a high amount of generation capacity installed within an HVDC grid connected to the existing AC grids.

As HVDC grids based on MMCs present a new form of grid, there is no standard protection system, yet. Several fault clearing strategies based on HVDC circuit breakers or fault-blocking converters have been proposed [3]. Among the proposed strategies, selective protection concepts based on HVDC circuit breakers similar to AC line protection concepts promise to limit the fault consequences the most [4]. In recent years, these concepts have been analysed in detail with respect to both fault detection and fault clearing including the stresses imposed on the DC system's components [5,6].

With regard to the overall power system stability, however, the impact of contingencies in the HVDC grid and the resulting temporary power outage in the adjacent AC systems need to be taken into account as well. It has to be ensured that the faults in the DC system do not cause instabilities in the AC system. To this end an analysis of the complete HVDC fault handling sequence, including the system recovery after fault clearing, has to be undertaken. Based on existing knowledge on fault detection and clearing this paper therefore shifts the focus of the analysis to the DC voltage and active power flow recovery. In particular the impact of different opening times of HVDC circuit breakers on the DC voltage and active power flow and its recovery are investigated for protection strategies employing HVDC circuit breakers at each line end in a variation of fault scenarios.

Section 2 outlines the investigated four-terminal HVDC system, the examined fault cases and the methodology used to analyse the recovery process. In section 3, the impact of different fault scenarios is analysed in detail for exemplary fault cases and a summary is given taking into account all investigated fault cases. Thereafter, the identified impact factors are summarised in section 4.

2 Investigation Methodology

2.1 System layout

The investigations are carried out in a four-terminal HVDC system specified in the Horizon 2020 project PROMOTioN, as shown in Figure 1.

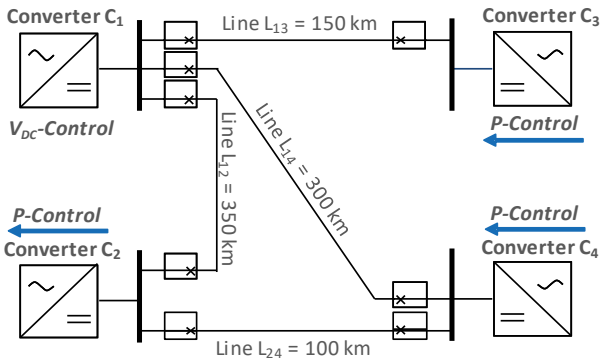

Figure 1: Investigated four-terminal system

Based on existing offshore windfarm connections, MMCs with half-bridge submodules are applied and the system is in symmetric monopole configuration with a high impedance star point reactor on the AC-side [2]. The lines are submarine XLPE cable connections with different line lengths, as given in Figure 2. The AC systems are represented by ideal sources with respective short circuit impedances (S_k = 30 GVA). For the studies in this paper, the converters C_3 and C_4 are considered to be offshore systems feeding in active power at their maximum capacity of $P_{c3} = P_{c4} = 1.2$ GW in P-control mode. C_1 is in V_{DC}-control mode, while C_2 is in P-control exporting $P_{c2} = 1.2$ GW. All converters are in V_{AC}-control mode. The used cascaded vector control is based on the work of Cigré WG B4.57 [7]. Table 1 summarises the main system parameters.

Parameter	*Rating*
Rated station power	1256 MVA
Rated active station power	1200 MW
Rated DC pole voltage	±320 kV
Rated AC voltage at MMC	350 kV
Rated DC pole current	1.875 kA
Number of submodules per arm	350
Rated submodule voltage	1.9 kV
Submodule capacitance	8.8 mF
Arm resistance	80 mΩ
Arm inductance	42 mH
Converter output inductance	10 mH
Star point reactor	5000 H, 5 kΩ

Table 1: Converter station parametrisation

The submodule parameters are based on an INFINEON IGBT commercially available with a continuous DC collector current of $I_{CDC} = 1.5$ kA and a collector-emitter voltage of $v_{CES} = 3.3$ kV [8]. The converter model is a *Type 4 Detailed Equivalent Circuit Model*, which enables an accurate representation of the converter's behaviour during faults [7]. The cables are modelled using a frequency dependent phase model for accurate representation of travelling wave phenomena [7]. The simulations are carried out with a simulation time step of $t_{step} = 4$ µs.
Within this system, faults are simulated at every line end, at a distance of 10 km from each line end, and in the middle of each line. The considered fault types are pole-to-ground and pole-to-pole-to-ground faults with a fault resistance of $R_f = 0.01$ Ω. For symmetry reasons only positive-pole-to-ground-faults are shown in this paper.

2.2 Fault clearing sequence

Figure 2 summarises the stages of an overall fault handling sequence based on HVDC circuit breakers for multi-terminal HVDC grids. After the fault incident, travelling waves propagate through the system. At the line ends, protection relays are used to detect the fault and trip the breakers on the faulted line selectively. Common detection criteria are based on the voltage breakdown and current rise. Due to the limited current breaking capability of the IGBTs within the converter and the proposed HVDC circuit breaker concepts, fault detection and clearing must be accomplished within a few milliseconds to ensure the safety of the system's components [9]. After successful fault clearing, the voltage in the system needs to be restored to its nominal value and the power flow has to be adjusted to the new system configuration.

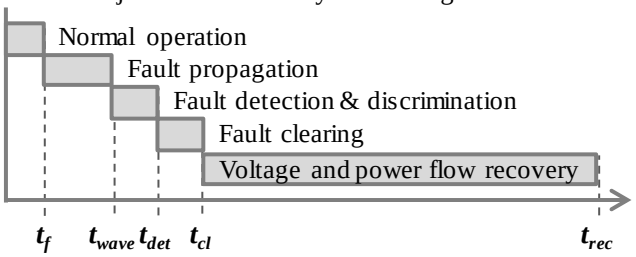

Figure 2: General fault handling sequence

As the focus of this paper is on the recovery sequence after fault clearing, an idealised selective protection is applied. The circuit breakers installed at the ends of the faulty line receive a trip signal after the arrival of the travelling wave at t_{wave} plus an additional delay accounting for the measurement and fault detection process of $t_{det} = 500$ µs. Due to the symmetric monopole configuration, both poles are tripped regardless of the fault type. The circuit breakers are modelled as ideal breakers in parallel to a surge arrester with a rated voltage of $v_{arrester} = 1.2$ pu. Different circuit breaker types are represented by different breaker opening times in the given model. Within this paper, opening times of $t_{open,HCB} = 2$ ms and $t_{open,SSCB} = 0.02$ ms are considered representing fast hybrid circuit breakers (HCB) and solid-state circuit breakers (SSCB) [10]. While hybrid circuit breakers are considered in most publications due to their low on-state losses, high fault current breaking capability and low breaker opening times, the choice of solid-state circuit breakers, which feature high on-state losses and lower current breaking capability, but very fast breaker opening times, serves to show the fastest possible recovery for the given system. To limit the fault current's rate of rise due to the fast cable discharge, inductors are installed at each line end with $L = 50$ mH. This ensures that the current breaking capabilities of the respective circuit breakers with $i_{max,SSCB} = 5$ kA and $i_{max,SSCB} = 16$ kA are not exceeded [10].
The converters have an internal overcurrent protection which blocks the IGBTs when the arm current exceeds 0.9 pu of the repetitive peak current of the IGBTs (here, $i_{arm,max} = 2.7$ kA). Assuming a fast de-blocking sequence, the IGBTs are de-blocked 1 ms after the overcurrent has subsided [9].
Due to the high impedance grounding on the AC side, pole-to-ground faults may lead to a voltage rise on the unaffected pole of up to $v_{pole,healthy} = 2$ pu. To alleviate this voltage unbalance, a dynamic breaking resistor (hereafter called chopper) is implemented at the terminal of C_1 [11]. It has a resistance of $R_{chopper} = 171$ Ω and is activated, if the voltage rises to $v_{pole} > 1.15$ pu. A hysteresis controller turns it off when the pole voltage falls below $v_{pole} < 1.09$ pu.

2.3 Analysis of system recovery

After fault clearing, the recovery of the DC voltage at each converter terminal and the power flow on the AC side are

evaluated. Depending on the affected line, the pre- and post-fault steady state can differ. Within this paper, the DC voltage is considered to be recovered when the voltage on each pole stays within ± 10 % of its nominal pole-to-ground voltage at all converter terminals. Similarly, the power flow is considered to be recovered when it is within ± 10 % of the power flow that results in steady state after the faulty line is separated from the system. The focus is set on the active power transfer at the point of common coupling on the AC side, for which the maximum deviation ΔP_{max} between the steady-state value after fault clearing and the largest or respectively smallest value is evaluated.

3 Results and Discussion

3.1 System recovery for solid-state circuit breakers

In Figure 3, the impact of fault clearing by SSCBs on the terminal voltage and current of C_1 is shown for an exemplary pole-to-ground fault in the middle of L_{12}. Note that the sign of the voltage of the negative pole has been inversed for scaling reasons. After the fault incident at $t_F = 0$ ms, the travelling waves reach the busbar and the voltage declines. The converter capacitors start to discharge and the current flow starts reversing towards the fault location. However, due to fast SSCB operation 520 µs after travelling wave impact, the fault is cleared before the pole voltage at C_1 breaks down entirely and the converter does not block. A steep voltage step occurs due to the breaker's transient interruption voltage. After breaker opening, the energy in the faulty line is discharged via the parallel surge arrester until the fault is cleared. After the clearing, the voltage at the converter terminal of C_1 stays within the defined voltage band as indicated by the dotted lines. This deserves special attention, because the prospective fault behaviour of symmetric monopole configurations with high impedance grounding typically leads to a rise of the voltage of the unaffected pole to $v_{pole,} = 2$ pu. Due to the fast fault clearing, the voltage asymmetry does not build up. The voltages at the other converters located farther from the fault show a similar behaviour after fault clearing, such that the DC voltage in the overall grid is recovered at $t_{rec,v} = 2.5$ ms.

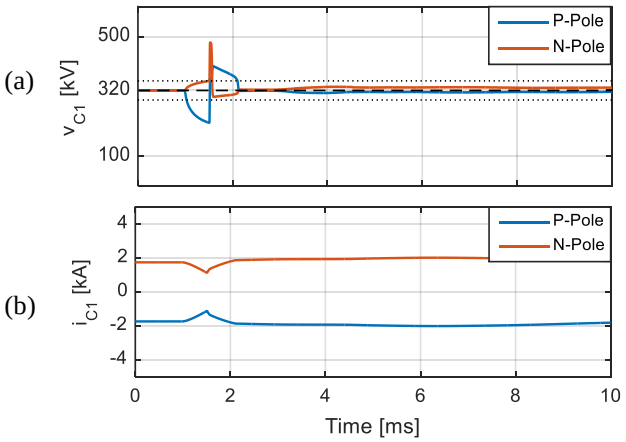

Figure 3: a) DC voltage and b) DC current at C_1 for a pole-to-ground fault in the middle of L_{12}

Figure 4 shows the active power on the AC side at all four converters for the same fault scenario in solid lines. There is no significant impact on the AC side power flow at any of the converters due to the fast fault clearing. A variation of the fault location on L_{12} has a significant impact on the voltage breakdown and the current rise within the DC system as known from previous studies [2]. However, the impact on the AC-side power flow stays the same as indicated for a fault 10 km from C_1 on L_{12} by the dashed lines.

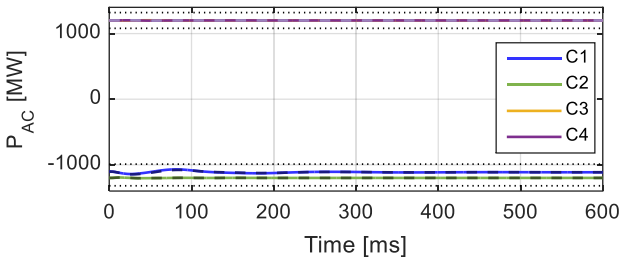

Figure 4: Active power at all converters for a pole-to-ground fault in the middle of L_{12} (solid lines) and a fault 10 km from C_1 on L_{12} (dashed lines) using SSCBs

In Figure 5, the power flow fluctuations at C_1 and C_2, representing the connection points to the onshore AC systems are shown for pole-to-ground faults on all lines. The curves are aligned based on the time the first travelling wave reaches the converter terminals to ease the comparison. As the fault location on each line has no significant impact, faults in the middle of each line are shown.

Depending on the affected line and the control mode of the converters the impact on the active power flow differs. The fault on the radial line L_{13} leads to the loss of power infeed from C_3, which gets disconnected, such that there is no further power export from the DC grid to the AC grid at C_1 after the line is isolated. C_2 is not affected by the fault and loss of C_3. Faults on L_{12} and L_{14}, which both only have marginal power flows due to the system layout before the fault occurs, lead to marginal power fluctuations at both converters.

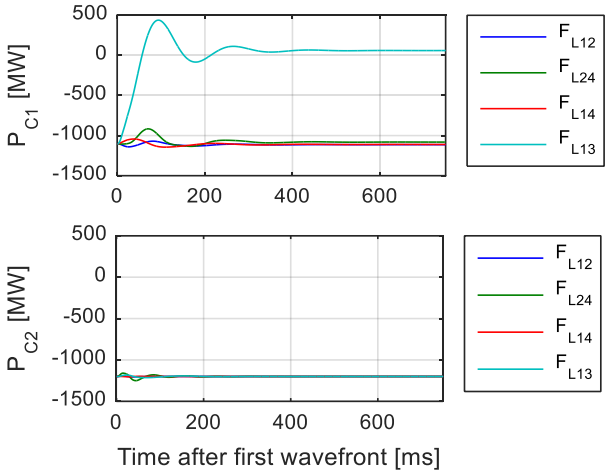

Figure 5: Active power at C_1 and C_2 for pole-to-ground-faults in the middle of each line using SSCBs

Faults on L_{24}, which exports the power from C_4 to C_2 lead to a maximum power deviation of $\Delta P_{max,C1} = 198$ MW at C_1 and

$\Delta P_{max,C2}$ = 48 MW at C_2. The latest system recovery is at $t_{rec,C1}$ = 113 ms. The impact on C_1, which is operating in V_{DC}-control mode, is slightly higher in comparison to C_2 in P-control mode. Overall the impact on the DC system and the AC power flow is limited due to the fast fault clearing. This also holds true for pole-to-pole-to-ground faults which are therefore not shown in detail for SSCB application.

3.2 System recovery for hybrid circuit breakers

The impact of a pole-to-ground fault in the middle of L_{12} on the voltage at C_2 using hybrid circuit breakers with and without the application of a DC-side chopper is shown in Figure 6.

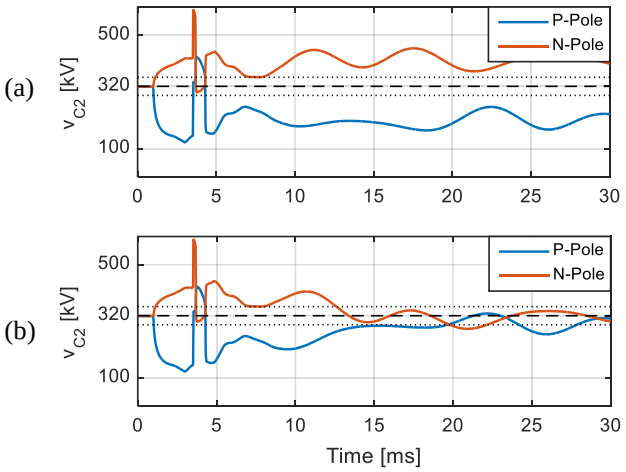

Figure 6: DC voltage at C_2 for a pole-to-ground fault in the middle of L_{12} a) without chopper and b) with chopper

In addition to the transient impact of the travelling waves at the converter terminals, a voltage asymmetry builds up before the fault is cleared. After fault clearing, the voltage asymmetry decays very slowly depending on the parasitic capacitance and resistance in the grid. Without the application of choppers, this leads to a voltage recovery at $t_{rec,v}$ = 420 ms. Applying the chopper leads to a faster discharge of the excess energy, such that voltage recovery is achieved at $t_{rec,v}$ = 28 ms. No blocking occurs for the analysed fault case. The impact on the AC-side power flow is shown in Figure 7 assuming chopper application. A significant impact can only be observed at C_1 with $\Delta P_{max,C1}$ = 350 MW and $t_{rec,C1}$ = 99 ms.

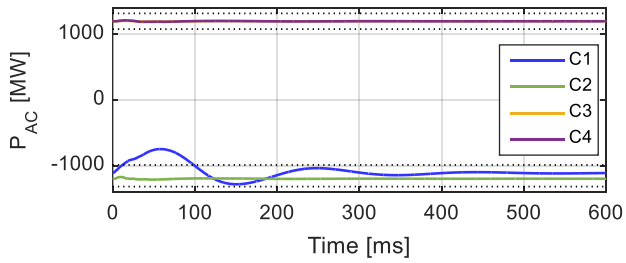

Figure 7: Active power at all converters for a pole-to-ground fault in the middle of L_{12} using HCB and choppers

Figure 8 summarises the active power fluctuations on the AC side for pole-to-ground faults in the middle of each line using hybrid circuit breakers and applying a chopper for voltage restoration. The effect of faults on the radial line L_{13} does not change in comparison to the scenario employing the SSCB as C_3 is disconnected from the system regardless of the breaker opening time. For faults on the other lines, however, the effect on the power flow increases. The maximum deviations at C_1 are $\Delta P_{max,C1}$ = 489 MW and the maximum recovery time is $t_{rec,C1}$ = 254 ms. The maximum deviation and recovery time at C_2 are $\Delta P_{max,C2}$ = 849 MW and $t_{rec,C2}$ = 147 ms.
In comparison to the fault clearing based on SSCB as shown in Figure 5, this is an increase of $\Delta P_{max,C1}$ = 291 MW and $\Delta P_{max,C2}$ = 801 MW. When comparing C_1 and C_2, there is a difference due to the control modes. The power flow at C_1 is influenced by all faults due to the V_{DC}-control mode. There is a higher impact in comparison to the fault clearance employing SSCB as the voltage breaks down further due to the longer breaker opening time of the HCB.
While in the previously analysed fault cases only marginal power flow deviations at C_2 occurred, there are now distinctive power flow deviations at C_2 for faults on L_{24} and L_{14}. This is due to a short-time blocking of C_2 in the given fault scenarios. The blocking leads to a power flow reversal at the point of common coupling as the connected AC grid starts feeding the fault current in the DC grid.

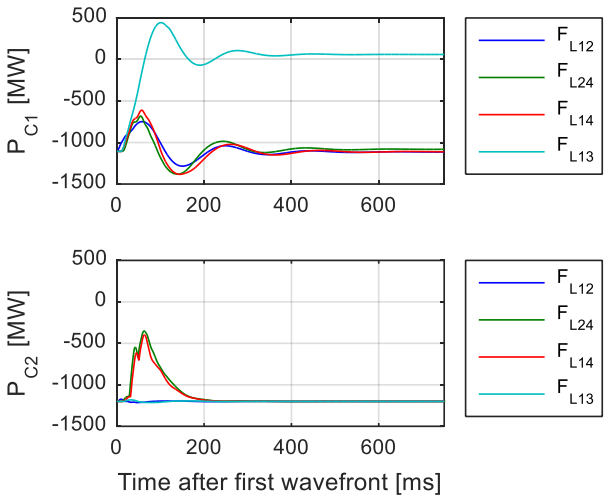

Figure 8: Active power at C_1 and C_2 for pole-to-ground-faults in the middle of each line using HCB and choppers

Figure 9 shows the DC voltage and current at C_1 for a pole-to-pole-to-ground fault in the middle of L_{12} using HCB for fault clearing. Due to the fault, the voltage on both poles at C_1 breaks down symmetrically and the current changes its direction reaching a maximum value of $i_{C1} > 4$ kA at the instant the breaker is opened. The fault current loop for pole-to-pole-to-ground faults consists of the converter arms, the corresponding line segments between the converter and the fault and the connection between the poles by the fault. The high impedance grounding on the AC side is not included in the fault current loop, such that no voltage asymmetry builds up. As a result, the DC voltage remains within the voltage band after the fault is cleared thus the voltage is recovered after $t_{rec,v}$ = 8 ms in the overall grid. In comparison to the fault clearance using SSCB, this is a few milliseconds slower. In

comparison to the pole-to-ground faults using HCB the voltage recovery is faster, as no voltage asymmetry builds up, which needs to be alleviated.

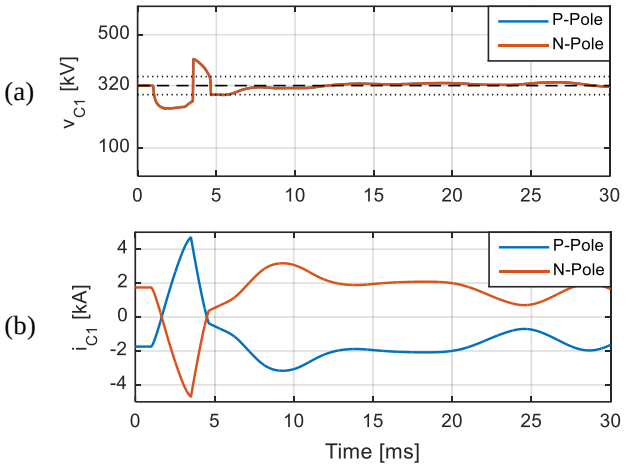

Figure 9: a) DC voltage, b) DC current at C_1 for a pole-to-pole-to-ground fault in the middle of L_{12}

Due to the voltage breakdown, the converter capacitors discharge and the maximum arm current amplitude in C_2 and C_4 rise to over $i_{arm,max} > 2.7$ kA before the breaker is opened. Subsequently, the converters block and de-block 1 ms after the maximum arm current has decayed below the threshold. The resulting impact of the fault clearing on the AC-side power flow is shown in Figure 10. Despite the longer fault clearing time and the blocking, C_3 and C_4 are only marginally affected, similarly to the previously shown fault scenarios. Overall this observation holds true for all investigated scenarios. The in-feeding converters C_3 and C_4 are the least affected, as there is no power flow reversal due to the faults. The exception being faults on L_{13}, which lead to the disconnection of C_3.

At the receiving converters C_1 and C_2, the maximum deviation of power flow and the recovery time for the investigated fault scenario are $\Delta P_{max,C1} = 208$ MW with $t_{rec,C1} = 170$ ms and $\Delta P_{max,C2} = 525$ MW with $t_{rec,C2} = 102$ ms respectively. The power flow deviations at C_2 result from the blocking of the IGBTs in this fault case.

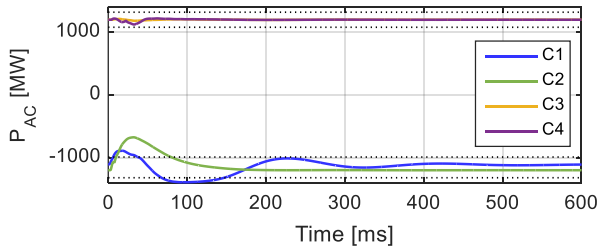

Figure 10: Active power at all converters for a pole-to-pole-to-ground fault in the middle of L_{12}

Figure 11 summarizes the resulting power flow fluctuations on the AC side for pole-to-pole-to-ground faults in the middle of each line. Again, the effect of faults on the radial line L_{13} does not change in comparison to the previously analysed scenarios. The application of the HCB leads to a maximum power flow deviation of $\Delta P_{max,C1} = 279$ MW at C_1 and $\Delta P_{max,C2} = 523$ MW at C_2. The power flow is recovered after $t_{rec,C1} = 165$ ms and $t_{rec,C2} = 110$ ms, respectively.

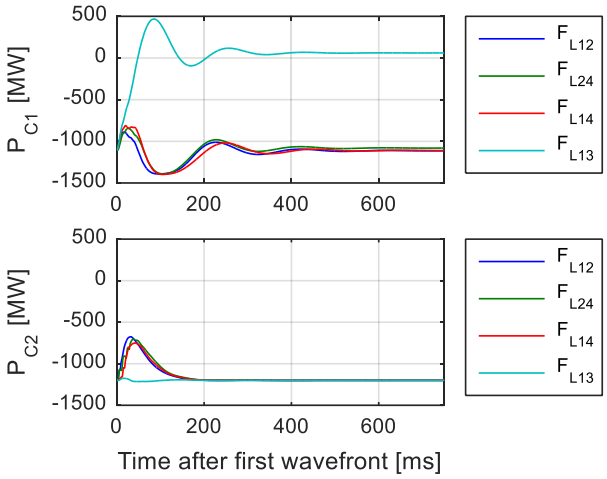

Figure 11: Active power at C_1 and C_2 for pole-to-pole-to-ground faults in the middle of each line using HCB

3.3 Direct comparison of active power flow recovery

To allow a direct comparison for the different fault types and circuit breaker opening times based on the previous results Figure 12 shows the power flow deviations at C_1 and C_2 for a fault in the middle of L_{24} for pole-to-ground (PGND) and pole-to-pole-to-ground (PNGND) faults using SSCB and HCB.

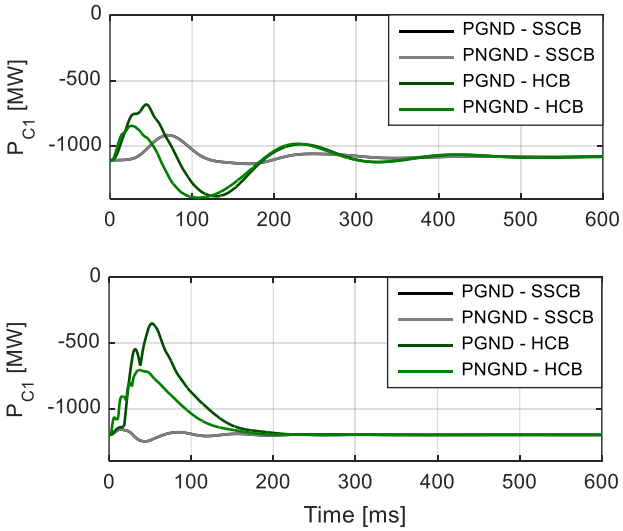

Figure 12: Active power at C_1 and C_2 for both fault types in the middle of L_{24} using SSCB and HCB and choppers

As was indicated by the previous results the fast fault clearance using SSCB leads to the lowest impact on the power flow. Moreover, there is no difference with regard to the fault type due to the fast fault clearing, thus the values for pole-to-ground-faults and pole-to-pole-to-ground faults are identical. Assuming the breaker opening delay of HCB, the impact on the power flow increases significantly. Furthermore, there is a difference between pole-to-ground and pole-to-pole-to-ground faults. The outlined need to alleviate

the voltage asymmetry after pole-to-ground faults leads to a higher impact on the AC side power flow, even though pole-to-ground faults are often reported to have less impact on the system due to the smaller resulting fault currents.

4 Conclusions

The planned integration of a high number of wind power plants using HVDC grids leads to new operational and protection challenges, which need to be considered with regard to the overall grid stability. As shown in the studied fault cases, the impact on the power transmitted to the AC system is marginal, if very fast solid-state based circuit breakers are used. However, solid-state based circuit breakers are often considered not applicable due to their high on-state losses. Hybrid circuit breakers, which feature mechanical switching elements, have breaker opening times of at least 2 ms, resulting in an impact on the AC system which is not negligible, even though a selective DC fault clearing strategy is employed. From the given analysis, the following aspects can be concluded:

- Faster fault separation leads to a smaller impact on the system and faster recovery of the power flow.
- The voltage recovery is completed a few milliseconds after fault clearing for pole-to-pole-to-grounds fault. If due to the breaker opening time a voltage asymmetry builds up for pole-to-ground faults, additional measures need to be taken to limit the voltage recovery time.
- The scenarios in which a rebalancing of the voltages after pole-to-ground faults is necessary lead to higher power flow deviations on the AC side.
- The impact on the power flow deviations depend on the control mode of the converter. Further studies are needed with regard to droop control and the tuning of the controllers.
- AC grids which transfer power into the DC grid are less affected, because no change of power flow direction occurs. Faults on L_{13} in the studied grid are an exception due to the complete disconnection of converter C_3.
- Blocking of converters which transfer power from the DC grid to the AC grid leads to a power flow reversal at the point of common coupling of the affected converter.
- The fault location on each line has a marginal impact on the AC-side power flow deviations. The location of the faulty line within the system has an impact depending on the pre- and post-fault power flow.

While the system under study represents a small system with only two wind farms and two onshore converters with a maximum power transfer of 2.4 GW to the onshore systems, there is already a distinctive effect on the power flow in the AC system for fast hybrid circuit breakers. Moreover, this paper analyses the power flow deviations at the point of common coupling to the AC grid from a DC-side perspective considering two asynchronous AC systems. In future grid scenarios, several converters will be connected to one synchronous AC grid zone like the continental European grid or the British grid, such that power flow deviations at both converter stations will have an impact on the same AC grid.
To be able to give an evaluation of the overall power flow deviations and their impact on the AC system, a detailed representation of the dynamic behaviour of AC systems is needed.
Future work will include the study of the power flow outage in larger HVDC grid structures. Within such topologies, a droop control approach will most likely be used, which will lead to power sharing between the converters in case of a fault and might ease the impact on single converter stations.

Acknowledgements

The authors' work has received funding from the European Union´s Horizon 2020 research and innovation program under grant agreement No. 691714.

References

[1] WindEurope. "Offshore Wind in Europe – Key trends and statistics 2017, windeurope.org, (2018).
[2] D. Van Heertem, O. Gomis-Bellmunt, J. Liang. "HVDC Grids – For Offshore and Supergrid of the Future", Wiley-IEEE Press, (2016).
[3] W. Leterme, D. Van Hertem. "Classification of fault clearing strategies", *Cigré Conference Lund*, (2015).
[4] M. Abedrabbo, M. Wang, P. Tielens; F.Z. Dejene, W, Leterme, J. Beerten, D. Van Hertem. "Impact of DC grid contingencies on AC system stability", *13th IET International Conference on AC and DC Power Transmission*, Manchester, UK, (2017).
[5] I. Jahn, N. Johannesson, S. Norga. "A survey of method for selective DC fault detection in MTDC grids", *13th IET International Conference on AC and DC Power Transmission*, Manchester, UK, (2017).
[6] N. A. Belda, C. A. Plet, R. P. P. Smeets. "Analysis of Faults in Multiterminal HVDC Grid for Definition of Test Requirements of HVDC Circuit Breakers", *IEEE Transactions on Power Delivery*. **33 (2)**, pp. 403-411, (2018).
[7] CIGRÉ WG B4.57. "Guide for the Development of Models for HVDC Converters in a HVDC Grid", *Technical Brochure 604*, (2014).
[8] Infineon Technologies AG. "FZ1500R33HE3 - IHM-B module with fast Trench/Fieldstop IGBT3 and Emitter Controlled 3 diode", IGBT Technical Information V 3.2, (2018).
[9] K. Sharifabadi, L. Harnefors, H.-P. Nee, S. Norrga, R. Teodorescu. "'Design, Control, and Application of Modular Multilevel Converters for HVDC Transmission Systems", Wiley-IEEE Press, (2016).
[10] M. K. Bucher, M. M. Walter, M. Pfeiffer, C. M. Franck. "Options for Ground Fault Clearing in HVDC Offshore Networks", *Energy Conversion Congress and Exposition*, pp. 2880-2887, (2012).
[11] G. P. Chaffey. "The Impact of Fault Blocking Converters on HVDC Protection", *PhD Thesis at Imperial College London*, (2016).